The challenge of simulating the sensitivity of the Amazonian clouds microstructure to cloud condensation nuclei number concentrations

Pascal Polonik[1,*], Christoph Knote[1], Tobias Zinner[1], Florian Ewald[2], Tobias Kölling[1], Bernhard Mayer[1], Meinrat O. Andreae[3,4], Tina Jurkat-Witschas[4], Thomas Klimach[4], Christoph Mahnke[5,6], Sergej Molleker[5], Christopher Pöhlker[4], Mira L. Pöhlker[4], Ulrich Pöschl[4], Daniel Rosenfeld[7], Christiane Voigt[2,6], Ralf Weigel[6], and Manfred Wendisch[8]

[1]Meteorologisches Institut, Ludwig Maximilians-Universität München, Munich, Germany
[2]Institut für Physik der Atmosphäre, Deutsches Zentrum für Luft- und Raumfahrt (DLR), Oberpfaffenhofen, Germany
[3]Scripps Institution of Oceanography, University of California at San Diego, La Jolla, California, USA
[4]Multiphase Chemistry and Biogeochemistry Departments, Max Planck Institute for Chemistry, Mainz, Germany
[5]Particle Chemistry Department, Max Planck Institute for Chemistry, Mainz, Germany
[6]Institut für Physik der Atmosphäre, Johannes Gutenberg-Universität, Mainz, Germany
[7]Institute of Earth Sciences, Hebrew University of Jerusalem, Jerusalem, Israel
[8]Leipziger Institut für Meteorologie, Universität Leipzig, Leipzig, Germany
[*]*now at:* Scripps Institution of Oceanography, University of California at San Diego, La Jolla, California, USA

Correspondence: Christoph Knote (christoph.knote@physik.uni-muenchen.de)

Abstract. The realistic representation of cloud-aerosol interactions is of primary importance for accurate climate model projections. The investigation of these interactions in strongly contrasting clean and polluted atmospheric conditions in the Amazon area has been one of the motivations for several field observations, including the airborne Aerosol, Cloud, Precipitation, and Radiation Interactions and DynamIcs of CONvective cloud systems - Cloud Processes of the Main Precipitation Systems in Brazil:

5   A Contribution to Cloud Resolving Modeling and to the GPM (Global Precipitation Measurement) (ACRIDICON-CHUVA) campaign based in Manaus, Brazil in September 2014. In this work we combine in situ and remotely sensed aerosol, cloud, and atmospheric radiation data collected during ACRIDICON-CHUVA with regional, online-coupled chemistry-transport simulations to evaluate the model's ability to represent the indirect effects of biomass burning aerosol on cloud microphysical properties (droplet number concentration and effective radius).

10   We found agreement between modeled and observed median cloud droplet number concentrations (CDNC) for low values of CDNC, i.e., low levels of pollution. In general, a linear relationship between modeled and observed CDNC with a slope of two was found, which means a systematic underestimation of modeled CDNC as compared to measurements. Variability in cloud condensation nuclei (CCN) number concentrations and cloud droplet effective radii (r_{eff}) was also underestimated by the model.

15   Modeled effective radius profiles began to saturate around 500 CCN per cm^3 at cloud base, indicating an upper limit for the model sensitivity well below CCN concentrations reached during the burning season in the Amazon Basin. Regional background aerosol concentrations were sufficiently high such that the additional CCN emitted from local fires did not cause a notable change in modelled cloud microphysical properties.

20 In addition, we evaluate a parameterization of CDNC at cloud base using more readily available cloud microphysical properties, aimed at in situ observations and satellite retrievals. Our study casts doubt on the validity of regional scale modeling studies of the cloud albedo effect in convective situations for polluted situations where the number concentration of CCN is greater than $500 \ \mathrm{cm}^{-3}$.

1   Introduction

25 Aerosol particles influence the formation of cloud droplets, and thereby the microphysical and macrophysical properties of clouds. Cloud droplet sizes and number concentrations determine the effect of clouds on atmospheric radiation and, therefore, also on weather and climate. Increased aerosol concentrations increase the cloud albedo (Twomey, 1991) and possibly the lifetime (Albrecht, 1989) of clouds by decreasing droplet size if the total liquid water mass is assumed constant. These indirect effects lead to increased cloud albedo and, thus, enhanced reflection of solar radiation under high aerosol loading, and therefore
30 causes a net cooling of the sub-cloud layer. However, the magnitude of these effects is not well constrained, which causes major uncertainties in current climate projections (IPCC, 2014).

Representing aerosol-cloud interactions in numerical models that form the basis of these projections is challenging because two of the most dynamic and complex atmospheric systems (aerosol and clouds) must be adequately represented individually before considering an accurate representation of their interactions. Multiple processes are involved, such as activation of aerosol
35 particles to cloud droplets, phase-transfer, evaporation, and wet deposition. Parameterizations with varying levels of complexity have been incorporated into numerical models of the atmosphere (e.g., Thompson et al., 2008; Morrison et al., 2005), which has led to improved short-term forecasts in certain case studies (Zhang et al., 2010). It is difficult, however, to disentangle benefits in forecast-relevant quantities (e.g., 500 hPa pressure field deviation or storm track accuracy) from an actual improvement in the modelled cloud macro- and microphysical characteristics and its impact on the atmospheric radiation budget. Testing
40 such parameterizations on a mechanistic level requires direct comparisons of model output to a variety of data sources (Seinfeld et al., 2016) as well as situations in which a noticeable aerosol signal can be expected. Events like volcanic eruptions (Malavelle et al., 2017; McCoy and Hartmann, 2015), desert dust outbreaks (Levin et al., 2005; Sassen et al., 2003), or wildfires (Rosenfeld, 1999; Brioude et al., 2009) provide strong signals that facilitate such process-level analysis of aerosol-cloud interactions.

In this work we present a case study that uses simulations and novel measurements of a recent field campaign to explore
45 aerosol-cloud-radiation interactions during the biomass burning season in the Amazon region. The Aerosol, Cloud, Precipitation, and Radiation Interactions and DynamIcs of CONvective cloud systems - Cloud Processes of the Main Precipitation Systems in Brazil: A Contribution to Cloud Resolving Modeling and to the GPM (Global Precipitation Measurement) (ACRIDICON-CHUVA) field campaign (Wendisch et al., 2016) was conducted over the Amazon in September 2014 during the dry season, when biomass burning from regional agricultural practices creates strong perturbations of cloud condensation

50 nuclei (CCN) number concentration (Pöhlker et al., 2018). We use remote sensing and in situ data collected by the High Altitude and Long Range Research Aircraft (HALO), operated by the German Aerospace Center (DLR) to evaluate our model predictions. Amongst other measurements, aerosol size and composition, CCN concentration, cloud phase and droplet size, and trace gas concentrations were collected. HALO flew underneath and within clouds to reconstruct vertical profiles. Typically, HALO research flights began with a ferry from Manaus to a region of interest and then back to Manaus (Figure 1, Table 1).

55 Regions of interest were areas with forecasted presence of convective clouds above specific surface conditions, such as intact forest or polluted agricultural burning areas. Many of the HALO flights were conducted in regions where medium or high aerosol number concentrations from biomass burning were suspected to influence cloud microphysical and radiative properties (Table 1).

We tried to reproduce the measurements conducted during the HALO flights by numerical simulations using the Weather

60 Research and Forecasting model with Chemistry (WRF-Chem, Grell et al., 2005) at convection-permitting scales. The simulations feature a size-resolved description of the full lifecycle of ambient aerosol, including biomass burning emissions, secondary particle formation through trace gas oxidation, and dry and wet deposition. Radiative properties of the aerosol population are considered based on size distribution and component-resolved optical properties (Barnard et al., 2010). The modeled aerosol description is linked to the detailed cloud microphysics parameterization of Morrison and Gettelman (2008). The num-

65 ber of CCN available for cloud formation as well as their physicochemical properties (size distribution and hygroscopicity) are provided to the cloud microphysics scheme based on the online-calculated aerosol properties. Conversely, activation of aerosol particles to cloud droplets leads to their removal from the aerosol-phase. Transport within cloud droplets, aqueous-phase chemistry, and washout by rain is explicitly represented in the model.

We first evaluate whether numerical simulations on convection permitting scales can accurately represent the observed

70 cloud microphysical properties. For this purpose we focus on cloud droplet number concentration (CDNC) and cloud droplet effective radius (r_{eff}) vertical profiles. r_{eff} profiles are representative of the microphysical development of a cloud and can be derived from in situ as well as remote sensing observations. Here we use in situ measurements of droplet size and number concentration along HALO flight tracks rearranged into profiles, and retrievals of r_{eff} profiles from passive remote sensing observations (Ewald et al., 2018).

75 While r_{eff} profiles describe the vertical evolution of cloud microphysical properties, it is actually the number of activated cloud condensation nuclei at cloud base, N_{a}, that provides the link between cloud development and aerosol availability. As N_{a} is a somewhat elusive quantity to observe, especially from satellites, parameterizations have been suggested to determine N_{a} based on observations of r_{eff} higher up in a cloud (Rosenfeld et al., 2012). In the second part of this work we evaluate the applicability of the parameterization from Freud et al. (2011) using in situ, remote-sensing and model-derived r_{eff} profiles.

Table 1. Dates of flights conducted during the ACRIDICON-CHUVA campaign, with basic information about each flight compiled from Wendisch et al. (2016) and the campaign blog (https://acridicon-chuva.weebly.com/; last accessed: July 10, 2018). CCN levels during each research flight are binned into low ("+"), medium ("++") and high ("+++").

Date	Flight #	CCN level	Description
2014-09-11	AC09	+	Clean conditions for cloud profiling
2014-09-12	AC10	+	Satellite coordination and several in situ clouds sampled in relatively clean conditions
2014-09-16	AC11	++	Tracer experiment near Manaus, with some fires in the vicinity
2014-09-18	AC12	+++	Polluted conditions but relatively few large clouds sampled
2014-09-19	AC13	+++	Polluted conditions, sampling of complete cloud profiles
2014-09-21	AC14	++	Satellite coordination, GoAmazon GI aircraft coordination, medium pollution
2014-09-23	AC15	++	Surface albedo measurement early, cloud sampled later, medium pollution
2014-09-25	AC16	++	Tracer experiment near Manaus, fires in the vicinity
2014-09-27	AC17	+++	Sample clouds over different land surfaces, compare to GPM satellite, polluted conditions
2014-09-28	AC18	+	Medium sized cumulus samples and full cloud profiles in clean conditions

2 Methods

2.1 Model

The Weather Research and Forecast model with Chemistry (WRF-Chem, Grell et al., 2005) was used to simulate atmospheric motion while incorporating online calculations of trace gases and aerosol physical and chemical processes in a nested domain setup. We used the Model for OZone And Related chemical Tracers (MOZART) gas-phase chemistry (Emmons et al., 2010; Knote et al., 2014) and the Model for Simulating Aerosol Interactions and Chemistry (MOSAIC) aerosol module (Zaveri et al., 2008), with a volatility basis set parameterization for organic aerosol evolution (Knote et al., 2015). Anthropogenic emissions data were taken from the Emissions Database for Global Atmospheric-Research from the task force for Hemispheric Transport of Air Pollution (EDGAR-HTAP, Janssens-Maenhout et al., 2012). Biogenic emissions are calculated online using the Model of Emissions of Gases and Aerosols from Nature (MEGAN, Guenther et al., 2006). The Fire Inventory from NCAR (FINN) module was used for the fire emissions data (Wiedinmyer et al., 2011). One degree resolution, six-hourly updated meteorological boundary conditions were taken from analyses of the National Center For Environmental Prediction Global Forecast System (NCEP GFS), and chemical boundary conditions were provided by forecasts of the global chemistry model MOZART (https://www.acom.ucar.edu/wrf-chem/mozart.shtml, last accessed February 6th, 2018). Cloud microphysical properties were represented by the double-moment microphysics scheme by Morrison et al. (2009), and no convection parameterization was applied in the nested domain. The Morrison scheme has five hydrometeor classes (cloud droplets, rain, cloud ice, snow, and

graupel), with each size distribution parameterized by a Gamma function. The cloud droplet effective radius is calculated through integration over the droplet size distribution:

$$r_{eff} = \frac{\int_0^\infty r^3 N(r)\mathrm{d}r}{\int_0^\infty r^2 N(r)\mathrm{d}r} \tag{1}$$

with r cloud droplet radius, and $N(r)$ droplet number concentration at radius r.

100   Effects of aerosol particles on atmospheric radiation (direct effect) are considered as presented in Fast et al. (2006). Activation of aerosol particles as cloud droplets is calculated based on the aerosol size distribution and chemical composition using κ-Koehler theory (Abdul-Razzak and Ghan, 2000, 2002), with relevant aspects of the implementation in the version of WRF-Chem used here presented in Gustafson Jr et al. (2007) and Chapman et al. (2009). The life cycle of activated aerosol particles is modelled explicitly; i.e., they are removed from the interstitial aerosol population and their evolution is modelled

105   in accordance with that of the cloud droplets in which they are incorporated in, including processes like washout from precipitation or re-evaporation. Cloud chemistry and limited heterogeneous processes are included as presented in Knote et al. (2015). Chemistry and aerosol processes are included in an operator-splitting fashion, in which individual processes update model fields sequentially. In each WRF-Chem time step, first advection is calculated, followed by droplet activation and finally the remaining chemistry and aerosol processes.

110   WRF-Chem simulations over the Amazon region were conducted for the ACRIDICON-CHUVA mission period between 8 - 30 September 2014. A continuous simulation with 15 km horizontal resolution, covering an area of approximately 3000 $\times$ 2700 km^2 (200 $\times$ 180 grid points), and 36 vertical levels up to 50 hPa, was conducted for the full campaign period (see Figure 1 for domain overview). To keep the large-scale meteorology in line with reality, WRF-Chem was restarted every 24 hours (at 0 hours UTC) from GFS analyses. Concentrations of trace gases and aerosol quantities were carried over, however,

115   to allow for multi-day pollution build-up and aging. Each 24 hour period was simulated with a 6 hour meteorological spin-up with nudging and a chemical restart file from the previous day. Meteorology was then allowed to evolve freely within the WRF-Chem domain (i.e. no nudging was applied) to enable the model to develop the implemented aerosol-cloud-interactions. Three additional days before the study period were simulated to spin-up trace gas chemistry and aerosol.

Convection-permitting, 3 km horizontal resolution domains (180 $\times$ 180 grid points, approx. 540 $\times$ 540 km^2) were then

120   "nested" into this simulation during days with HALO flights. Two-way interactions were allowed between the parent and the nested domains. The location of these "nests" varied and were chosen so that they covered the area of interest sampled by HALO in each flight (Figure 1, see also Section 3.1). On each flight day, the nested domain was started (by interpolating the current state of the outer domain) at 09:00 UTC and run until 21:00 UTC, hence covering the full time frame of each HALO research flight. All model results presented in this study are from the nested, convection-permitting domains.
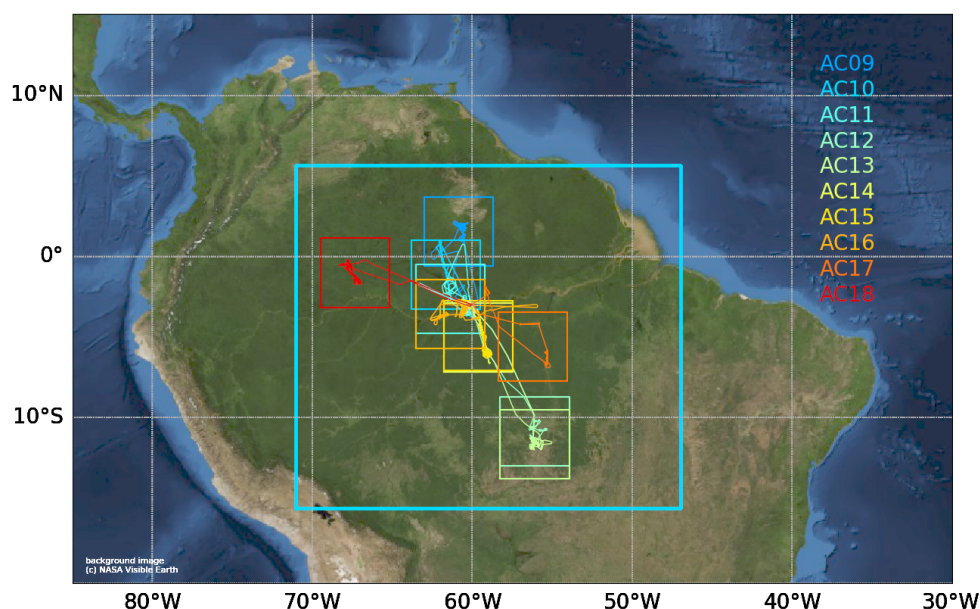
Figure 1. A map showing the campaign area, with all ACRIDICON-CHUVA research flights considered in this study as color-coded lines, the continuously-run outer simulation domain (blue box) as well as the individual nested domains used for analysis of each research flight, identified by the flight labels (Table 1).

2.2 Measurements

2.2.1 Cloud in situ measurements

The cloud combination probe (CCP) combines the cloud imaging probe (CIP) and the cloud droplet probe (CDP) to measure the cloud particle size distribution by detecting their forward-scattered laser light (Lance et al., 2010). During the ACRIDICON-CHUVA campaign, the CCP measured at 1 Hz frequency from underneath the right wing of the HALO aircraft (Wendisch et al., 2016). A correction for the high flight velocities was applied to improve data quality (Weigel et al., 2016). The CCP measures particles with diameters between 2 - 960 µm, but here we only used the 14 bins for particle diameters from 3 - 50 µm (from the CDP) to calculate the cloud particle effective radius. Except for the details of the selection of appropriate data points, the data used here is the same as described in Braga et al. (2017a). To filter the data we calculated liquid water content from binned effective diameter measurements and only included those with at least $1 \, \mathrm{g \, kg^{-1}}$ liquid water content. This threshold is consistent with the one used to define "cloudy" points in model output.

Like the CCP-CDP, the Cloud and Aerosol Spectrometer with Depolarization (CAS-DPOL) measures cloud particle size distributions at 1 Hz frequency (Baumgardner et al., 2011; Voigt et al., 2017). The CAS-DPOL measures the intensity of

forward-scattered light between 4 - 12 degrees in 30 size bins from particles with diameter 0.5 - 50 μm. The polarized backward-scattered light is used to analyze the sphericity and thermodynamic phase of the measured particles (Baumgard-
140 ner et al., 2014; Järvinen et al., 2016), but this capability was not used for our analysis. Our calculation of the cloud particle effective radius (Schumann et al., 2017) was again limited to particles between 3 - 50 μm, which corresponds to 10 Mie-ambiguity corrected size bins, to account for consistency with the CDP. Further details on CAS-DPOL data evaluation are given in Kleine et al. (2018).

Profiles of r_{eff} were derived using data from both the CAS-DPOL and the CDP. Braga et al. (2017a) demonstrated that
145 the CDP and CAS-DPOL instruments are comparable within their expected measurement uncertainties. Flamant et al. (2018) and Taylor et al. (2019) also found good agreement between CAS-DPOL and CDP measurements in shallow clouds. Here, we combine measurements from both instruments into one in situ dataset to construct effective radii profiles. Therefore, the concentration of activated cloud condensation nuclei N_{a}, is derived using all in situ r_{eff} measurements with their respective adiabatic liquid water content (see further description in Section 2.2.4). Treating in situ measurements from the two instruments
150 as independent is justifiable in part because they are located on opposite wings of the aircraft.

2.2.2 CCN in situ measurements

The number concentration of CCN was measured with a continuous-flow streamwise thermal gradient CCN counter (CCNC, model CCN-200, DMT, Longmont, CO, USA) (Roberts and Nenes, 2005; Rose et al., 2008). Activated CCN that grow to a diameter of at least 1 μm at a set water vapor supersaturation between 0.1 - 5% are counted by the instrument at 1Hz. Two
155 sample inlets were used during the ACRIDICON-CHUVA campaign, but here we only use data from the HALO aerosol sub-micron inlet (HASI), which collected data at a constant supersaturation of 0.55 %. The uncertainty of the CCN measurements is dominated by the counting statistics and ranges between 10% for high CCNs and 20% for low CCNs (Krüger et al., 2014). The supersaturation uncertainty is also about 10% (Braga et al., 2017a).

2.2.3 Cloud remote sensing measurements

160 The spectral imager of the Munich Aerosol and Cloud Scanner (specMACS) was installed on the HALO aircraft during ACRIDICON-CHUVA. specMACS is a hyperspectral line camera that measures at visible and near-infrared wavelengths (Ewald et al., 2016). Marshak et al. (2006) and Martins et al. (2011) suggested using the solar radiation reflected by illuminated cloud sides to derive the vertical profile of effective radius and cloud phase, but the ACRIDICON-CHUVA campaign was the first time that passive cloud side remote sensing was applied systematically for a large number of cases. Zinner et al.
165 (2008) and Ewald et al. (2018) developed a cloud side retrieval and demonstrated the application using ACRIDICON-CHUVA data. Jäkel et al. (2017) derived phase information from cloud-side reflectivity measurements during ACRIDICON-CHUVA. specMACS was mounted on HALO at a sideward viewing port to observe clouds passed by the aircraft. Cloud vertical profiles were then retrieved using the method by Ewald et al. (2018) along the flight route akin to a push-broom satellite instrument. Results for three cases are compared to in situ and WRF-Chem model data.

170   specMACS cases shown in this paper are first example cases and mainly presented to showcase the capability of airborne remote sensing to provide effective radius profiles and cloud droplet number concentration (CDNC). They are not representative for whole flights or flight regions as the used in situ or modelled data, but show specific example local situations along a few minutes of flight time. In this respect they complement the large scale picture provided by modelled data averaged over 540×540 km^2 or the in situ data collected over several hours flight time. specMACS cloud scenes were selected based on

175   favorable data collection conditions. This includes minimal turning of the aircraft, favorable sunlight conditions, and high cloud coverage.

2.2.4   Derivation of N_a from in situ, remote sensing, and model cloud data

The central quantity to determine the influence of aerosol on cloud development and lifetime is the number of activated cloud condensation nuclei at cloud base, N_a. During ACRIDICON-CHUVA, HALO directly sampled N_a during their cloud profile

180   flights, providing a valuable comparison. As the collection of in situ data is expensive and spatial coverage is limited, Rosenfeld et al. (2012) suggested to infer N_a at cloud base using other more readily available observations like satellite retrievals. Freud et al. (2011) proposed a parametrization that derives N_a from the vertical profile of droplet radii. To do this, an adiabatic liquid water content (LWC_a) is calculated from cloud base pressure and temperature under the assumption that all water vapor above the saturation vapor pressure is condensed during the moist adiabatic ascent of a parcel at a fixed N_a can be derived using an

185   empirical relation between r_{eff} and the volumetric radius, r_v (i.e., $r_v = 1.08 \cdot r_{eff}$ as in Freud et al. (2011)), LWC_a, and the density of water ρ_w:

$$N_a = \frac{1}{\rho_w} \cdot \frac{3}{4\pi} \cdot \frac{LWC_a}{r_v^3} \cdot 0.7 \qquad (2)$$

The ratio of LWC_a and r_v^3 is found as the slope of a linear regression through all available point pairs of LWC_a and r_v^3 in the droplet size profile, forced through the origin. An additional mixing factor of 0.7 accounts for the imperfection of the adiabatic

190   assumption (Freud et al., 2011; Braga et al., 2017a). Freud et al. (2011) empirically derived this factor using in situ effective radius and LWC data from multiple previous field campaigns, including one in the Amazon. Although there was geographic diversity in the data used for the derivation, only one estimation was made which may introduce an unknown error in our studies. This could be especially relevant for remotely sensed data that measure cloud sides rather than a cloud cross-section. Nonetheless, we apply the same derivation and same mixing factor to all three available r_{eff} datasets: remotely sensed, in

195   situ, and model output. Applying this method to multiple data sources provides insights into the validity of this concept. The resulting N_a can also be used for direct comparison of the different input r_{eff} profiles.

3 Representation of cloud microphysics in the model

3.1 Deriving comparable quantities for model-measurement evaluation

Comparing the three different sources of information on cloud microphysical properties (model, remote-sensing, and in situ
observations) is not straightforward. Colocating in situ and remote-sensing observations required observing a cloud using
the side-facing specMACS, and then flying into this cloud to obtain respective in situ measurements. During ACRIDICON-
CHUVA, cloud clusters had been identified for each research flight, which were then passed several times to allow for remote-
sensing observations before probing these clusters in situ. This precludes direct comparison of individual clouds without
diligent data selection, but allows for a statistical comparison of in situ data collected near the cluster and the corresponding
remote-sensing observations. Simulations will not reproduce an individual (observed) cloud, but they will create a comparable,
realistic regional environment with comparable clouds. Hence, the nested domains were chosen such that they are center on
the cloud cluster chosen as target for an ACRIDICON-CHUVA research flight. Assuming a homogeneous environment within
the model domain, a statistical comparison of all modelled clouds in the model domain with observations taken of the cloud
cluster within the domain is reasonable. Therefore, we used all clouds within the respective nested model domain to derive
model statistics. Observation statistics are based on all data collected within the spatial domain of the model nest. As mentioned
above, statistics pertaining to in-cloud variables are restricted to data points with a liquid water content of more than $1 \, \mathrm{g \, kg^{-1}}$
in both model and observations.

3.2 Cloud droplet number concentrations

Figure 2 shows median in situ measurements of CDNC during flights and the median CDNC values from the entire nested
model domain corresponding to the flight. Modeled and measured CDNC match for lower values of 200 $\mathrm{cm^{-3}}$ (AC09), but
diverge for higher values. There is a linear relationship between WRF-Chem results and observations, albeit below the one-to-
one line, leading to a factor of two of underestimation of CDNC for the most polluted case investigated (AC12 with about 750
$\mathrm{cm^{-3}}$ observed).

3.3 Variability in modeled r_{eff} profiles

All WRF-Chem modeled r_{eff} data from the ten nested domains was combined and binned by cloud-base CCN concentration
(Figure 3). Cloud-base CCN is defined as the modeled CCN concentration at 0.5 % supersaturation directly below the lowest
cloudy pixel in a model column.

The binning of r_{eff} profiles shows that the modeled profiles correspond to theoretical expectations; clouds with more avail-
able CCNs have a r_{eff} profile that is shifted towards smaller values relative to those with less available CCNs. The response
to CCN concentration saturates in the model around 500-600 $\mathrm{cm^{-3}}$, indicating that biomass burning effects will be nonlinear
and strongest in relatively clean conditions. We did not find such a saturation effect for CDNC (Figure 2). Between 2 - 4 km
above sea level, where the most model clouds occur, the slope of the profile also scales with available CCNs. The radius grows
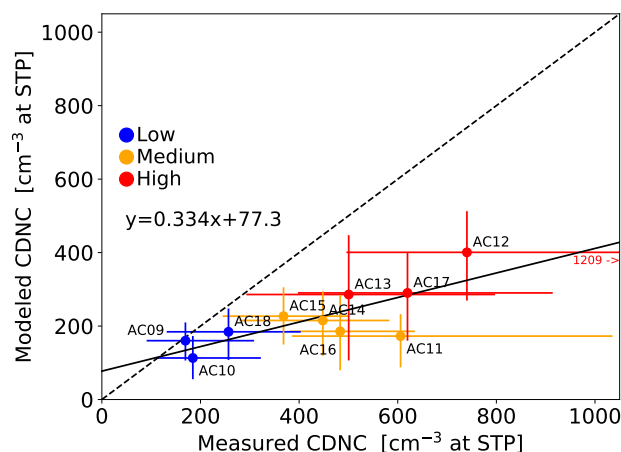
Figure 2. Median cloud droplet number concentration from the WRF domain and in situ measurements. The colors correspond to the CCN level labels in Table 1. Error bars depict the interquartile range (25 - 75% of all values). The equation describes the (solid black) regression line. The dashed black line is a 1-to-1 line for reference. STP refers to standard temperature (273.15K) and pressure (1000hPa).
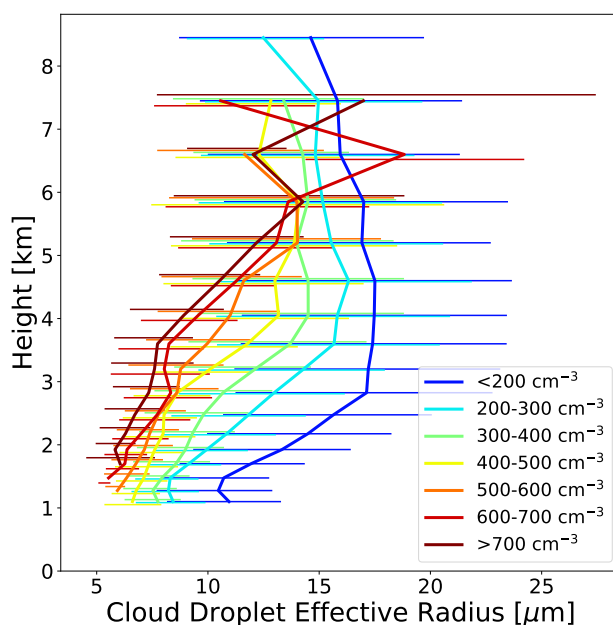

Figure 3. WRF-Chem simulated median cloud drop effective radius vertical profiles from all nested domain output during the study period, binned by below-cloud CCN concentration $[\mathrm{cm^{-3}\ at\ STP}]$. Error bars represent the 20th to 80th percentile for each level and are offset vertically for readability.
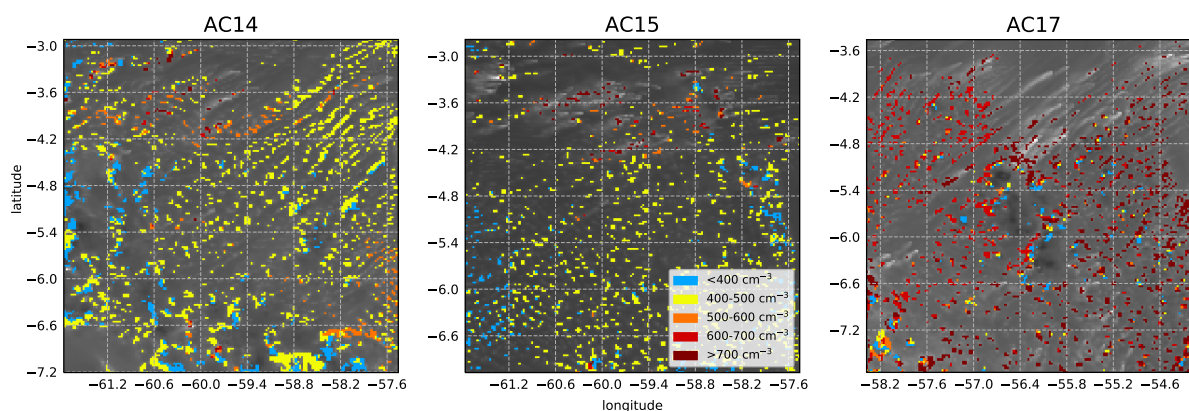
Figure 4. Spatial variability in modeled concentration of CCN at cloud base on three days (at 18Z) during the field campaign. Modelled aerosol optical depth (AOD) is shown as grey shading in the background, with brighter colors indicating higher AOD values.

quickly with height to a maximum r_{eff} under low CCN (clean) conditions, whereas under high CCN (polluted) conditions the radius does not reach a maximum until much higher in the atmosphere. The profiles reach a maximum and then remain roughly

230   constant at higher elevations. Under clean conditions, the maximum r_{eff} is larger and is reached at lower elevations. Profiles for the cleanest conditions also exhibit the largest maximum median r_{eff} of about 17 μm.

3.4   Comparison of modeled and observed r_{eff} profiles

WRF-Chem modelled r_{eff} profiles were compared to remote-sensed and in situ measured profiles. In Figure 4 we show snapshots of the spatial variability of modeled CCN concentrations at cloud base for three different days. Figure 5 a-c then shows

235   r_{eff} profiles derived from specMACS from two-minute cloud scenes on these three days, below-cloud-CCN binned WRF r_{eff} profiles from three hours near the specMACS data collection time, and all in situ r_{eff} profile measurements within the nested model domain. Figure 5 d-f shows the known modeled and in situ CDNCs. Being a remote-sensing technique, no CDNC are available for the specMACS observations.

Note that this is an approximate comparison, as no exact colocation can be expected between in situ and remote-sensed

240   clouds, and we cannot compare individual modelled clouds directly to observed ones. Visual inspection of the slope and magnitude of median r_{eff} profiles measured by specMACS suggests that they match reasonably well to those from WRF-Chem, though in situ r_{eff} tend to be smaller than both the modeled or the ones retrieved by specMACS for all three cases investigated here.
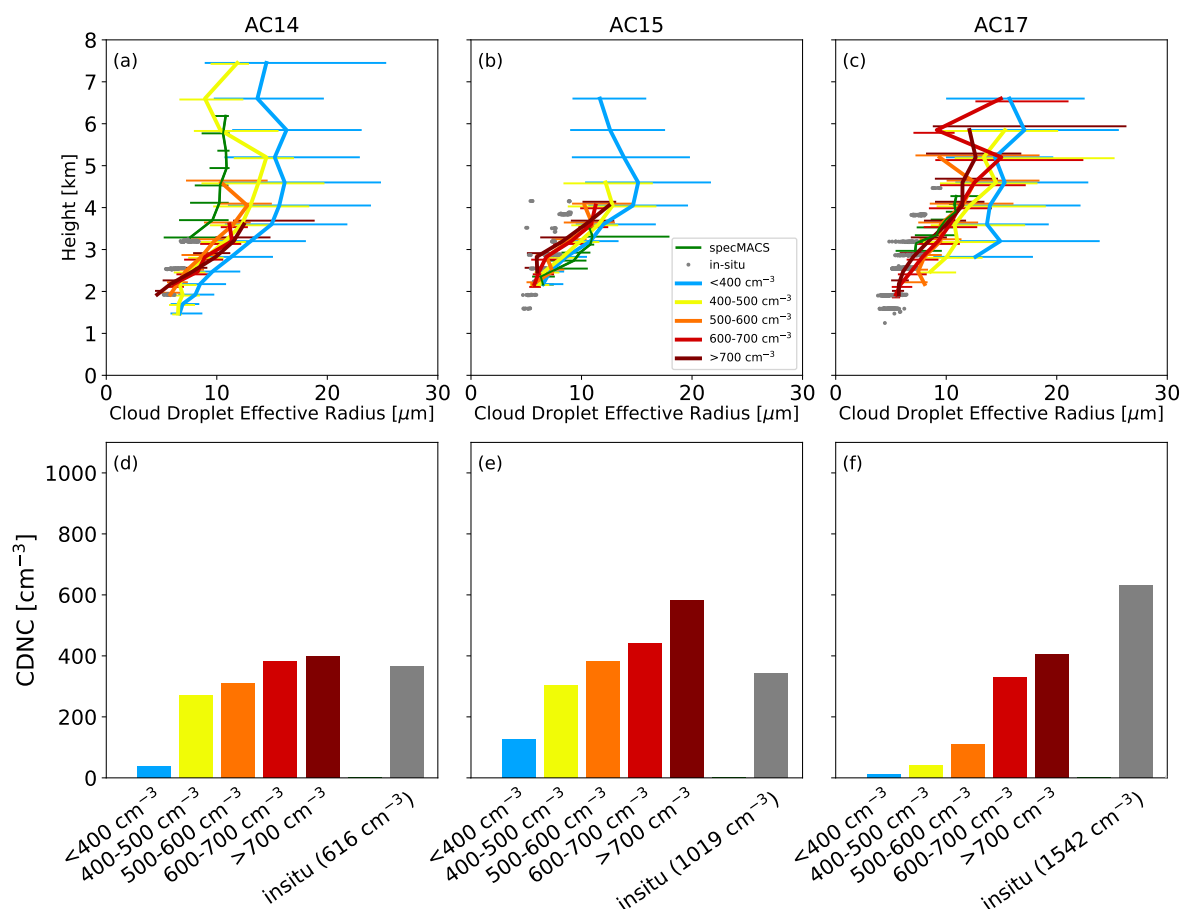
Figure 5. r_{eff} profiles and associated cloud droplet number concentration (CDNC) on three days during the field campaign. (a-c) show a comparison of median WRF-Chem, specMACS, and insitu r_{eff} profiles. (d-f) show the "true" below-cloud CCN-binned CDNC from WRF-Chem simulations and CDNC from in situ cloud profiling. Average in situ CCN concentrations (below 2 km) are presented in the bar label for the the in situ derived N_a. See Section 3.1 for details regarding the definition of "average".

3.5 Number of activated cloud condensation nuclei at cloud base

245 As a more quantitative comparison of the different profiles, the number of activated CCNs at cloud base (N_a) were derived for each profile based on the methodology proposed in Freud et al. (2011). For the same three days as in Figure 5, Figure 6 a-c shows the regressions between adiabatic liquid water content (LWC_a) and mean volume radius (r_v) that result (using Eq. 2) in the calculated $N_{a,calc}$ values shown in Figure 6 d-f. LWC_a for the modeled profiles was calculated in model clouds at the same points as used for the r_{eff} values. For specMACS, a nested domain averaged LWC_a profile was used since the

250 below-cloud CCN is unknown for those measurements. The same profile was used for the in situ LWC_a to allow for direct comparisons. Only the increasing portion of the WRF-Chem profiles were used for the fits in Figure 6 a-c; points above the

first decrease that occurs above 4 km are excluded. The known CDNCs (Figure 5) and calculated N_a (Figure 6) matched well given that CDNC is being viewed as equivalent to N_a, although N_a is an upper limit for CDNC since CDNC can be influenced by processes like collision and coalescence. A direct comparison of the true and derived CDNC are shown in Figure 7. This

255   comparison demonstrates the effectiveness of the Freud et al. (2011) method for model data. The relationship is linear, but there is a systematic positive bias of derived CDNC. The factor of 0.7 as taken from the literature may be an underestimation for the modeled clouds. Sensitivity of the derivation to cloud base height may explain why using modeled LWC_a resulted in high derived CDNC for two of the in situ derivations. Another contributor could be the high low-level CCN concentrations that were not reached in the model and in part by the use of an average model LWC_a rather than a "true" LWC_a. Even though $N_{a,WRF}$

260   and $N_{a,calc}$ do not match exactly, general trends are captured. The N_a derived from the specMACS r_{eff} profiles ($N_{a,spec}$) fall within the range of modeled CDNCs (Figure 6 d-f). Compared to modeled CDNCs, specMACS-derived $N_{a,spec}$ are relatively high, low, and central for AC14, AC15, and AC17, respectively.

With the available data it is not possible to know the aerosol or below-cloud properties for the clouds sampled by specMACS. We suggest, however, that we can use the model results to deduce that the specMACS observed relatively polluted clouds during

265   AC14 (Figure 6 a,d), relatively clean clouds during AC15 (Figure 6 b,e), and medium polluted clouds during AC17 (Figure 6 c/f). The N_a derived from the in situ profiles is higher than the others. While the calculated N_a depends on the theoretical adabatic liquid water content (LWC_a), the measured LWC might in fact be lower. This finding should be explored further but is out of scope of this work.

3.6   Discussion

270   Modeled r_{eff} tended to be larger than in situ measurements of r_{eff}. Subsequently, directly modeled and model-derived CNDC concentrations were lower than in situ measurements and derivations. Partly, these differences can be accounted for by the low modeled CCN concentrations (Figure 2). However, the 20th to 80th percentile range of modeled profiles with high below-cloud CCNs do overlap with the in situ data. The modeled r_{eff} profiles began to saturate around $500 \, \mathrm{cm}^{-3}$ at STP below-cloud CCN, with only small differences at higher concentrations (Figure 3), meaning that the modeled aerosol-cloud interactions saturate at

275   approximately that concentration. This concentration is well below the CCN concentrations characteristic of the dry season in the southern half of the Amazon Basin, which are typically in the range of 1000 to $7000 \, \mathrm{cm}^{-3}$ (Andreae et al., 2004; Andreae, 2009; Andreae et al., 2018). No such saturation was observed in the evaluation of modelled CDNC.

Increased model spatial resolution could potentially provide better agreement for these high-pollution situations, but a variety of hurdles (input data resolution of emissions and static data like land use, vegetation cover and topography, model formulation

280   of turbulence, statistical methods for output analysis) need to be overcome before reliable simulations at higher resolution are feasible. The horizontal grid resolution of 3 km is at the fine end of what regional modeling systems were designed for, reaching for 'terra incognita' (Wyngaard, 2004) in terms of resolution. Sensitivity simulations in which we simply increased the horizontal and/or vertical resolution by a factor of two did not lead to improved agreement with observations.

We deem our modeling study is representative for other regional scale chemistry-transport modeling studies of aerosol-cloud

285   interactions of convective clouds in situations strongly affected by biomass burning (e.g., Martins et al., 2009; Wu et al., 2011;
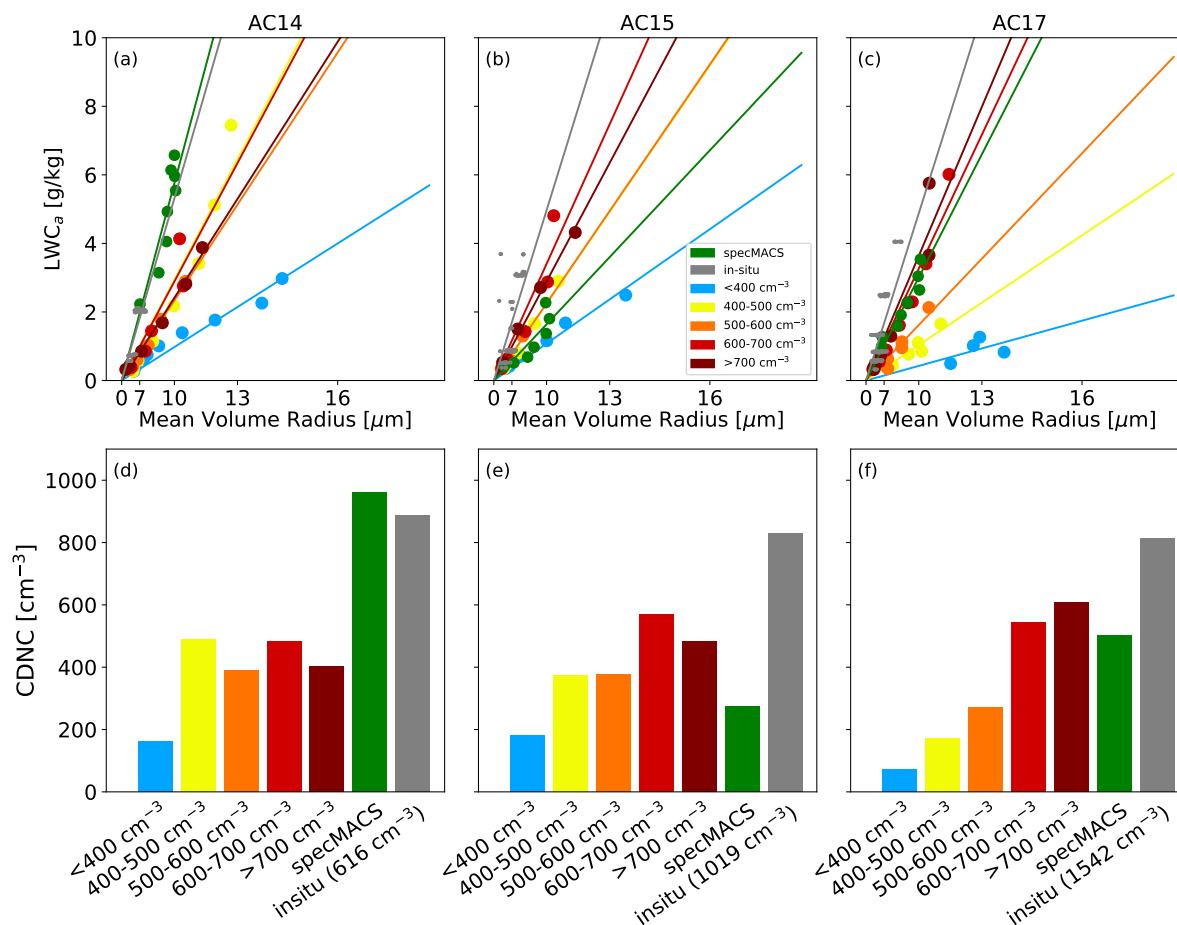
Figure 6. Derived cloud droplet number concentration (CDNC) on three days during the field campaign. (a-c) show the regressions between mean volume radius and adiabatic liquid water content (LWC_a) used to derive the CDNC as shown in (d-f). Average in situ CCN concentrations below 2 km are shown below the in situ derived N_a. (d-f) were derived from the slopes in (a-c), whereas Figure 5 d-f were more directly determined.

Archer-Nicholls et al., 2016). WRF-Chem is a widely used modeling system and similar to other regional modeling systems, our setup including a two-moment cloud microphysics scheme with a sectional aerosol module the current state of the art, as is the representation of aerosol-cloud interactions using the cloud activation scheme of Abdul-Razzak and Ghan (2000).

Comparisons between entire model domains and in situ measurements are inherently difficult since the exact measured clouds will never be realistically measured due to the randomness of modeled clouds and the difference in scales. There are a variety of challenges involved with this comparison. However, especially at high CCN, the model overestimates r_{eff} and, therefore, underestimates N_a. The specMACS data experience similar comparison difficulties since each set only spans a cloud scene ($\sim$50 km) over a short time ($\sim$2 minutes). However, the retrieved r_{eff} profiles still fall within the in situ measurements
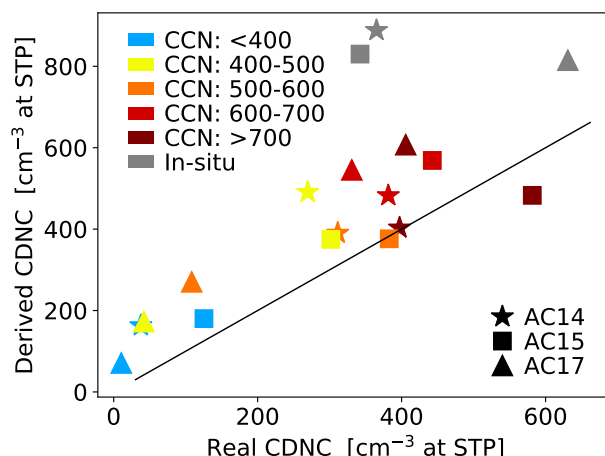
Figure 7. Comparison of real (i.e. CDP and CAS measured) CDNC with CDNC as derived using the Freud et al. (2011) method. Real CDNC for model data is average modeled CDNC in the model domain. Symbols indicate date, colors indicate model bin or in situ data. The one to one line is for reference. These are the same data as Figure 5 d-f and Figure 6 d-f.

and the model output. Profile values derived from specMACS measurements also tend to be smaller than the data from in situ
sampling, which is expected based on previous tests (Ewald et al., 2016).

We have demonstrated that the method by Freud et al. (2011) to derive cloud base CDNC from r_{eff} observations can successfully be applied in conjunction with simulated clouds to derive N_{a} from remotely sensed hyperspectral data of the specMACS
instrument. The method is limited by its high sensitivity at low N_{a} due to the mathematical nature of the slope (i.e. steep slopes
in Figure 6 a-c) and we are unable to verify its accuracy with the available data. It also uses an average mixing factor that may
vary for the cloud scenes measured my specMACS. However, using Figure 7 as a guide to the accuracy of the method, the
uncertainties appear to be smaller than those from satellite retrievals, which are about 78 % at the pixel level (Grosvenor et al.,
2018). We therefore propose that model results can be used to differentiate specMACS observations into clean and polluted
conditions, which will need to be verified in future studies.

4 Conclusions

Aerosol-cloud interactions have been the focus of field campaigns and measurement development due to the large associated
model uncertainty. Here we used novel observations taken on board of HALO during the ACRIDICON-CHUVA field campaign
to evaluate cloud representation in a numerical model to aid in reducing this uncertainty. We demonstrated that we can reproduce realistic cloud properties (i.e., cloud droplet effective radius profiles) with a regional online-coupled chemistry-transport
model at convection-permitting scales for the Amazon region during the biomass burning season. As expected by theory, the
number of CCN at cloud base has a major influence on cloud droplet size and the shape of the effective radius vertical profile. Increasing CCN leads to decreasing cloud droplet sizes, and we could show that both model and observations exhibit

Atmospheric
Chemistry
and Physics
Discussions

quantitatively similar behavior. We also observed a saturation effect at high aerosol concentrations (number concentration of CCN larger than 500 cm^{-3} at STP) in the model, above which we find no further change in modelled effective droplet size or the shape of the droplet size profile. This model result is in disagreement with observations of microphysical effects at much

315 higher aerosol loading from previous campaigns (Reid et al., 1999; Andreae et al., 2004) and from the ACRIDICON-CHUVA campaign (Braga et al., 2017b). This finding casts doubt on the validity of regional scale modeling studies of the cloud albedo effect (Twomey, 1991) of convective clouds for biomass burning situations where the number concentration of CCN is larger than 500 cm^{-3} at STP.

Code and data availability. Model data, the source code used in the evaluation, as well as all observational data, are available from the
320 authors upon request.

Author contributions. PP made the simulations and conducted the analysis under the supervision of CK and TZ. PP, TZ and CK wrote the manuscript, with input from BM, MA, DR, RW and MW. MA, CP, MP, UP, DR, RW and MW contributed through fruitful discussions. FE, TKo, TJ, TKl, CM, SM, CP, MP, CV and RW provided measurements essential for this manuscript.

Competing interests. The authors declare no competing interests.

References

335 Abdul-Razzak, H. and Ghan, S. J.: A parameterization of aerosol activation: 2. Multiple aerosol types, Journal of Geophysical Research: Atmospheres, 105, 6837–6844, https://doi.org/10.1029/1999JD901161, 2000.

Abdul-Razzak, H. and Ghan, S. J.: A parameterization of aerosol activation 3. Sectional representation, Journal of Geophysical Research: Atmospheres, 107, https://doi.org/10.1029/2001JD000483, 2002.

Albrecht, B. A.: Aerosols, cloud microphysics, and fractional cloudiness, Science, 245, 1227–1230, 1989.

340 Andreae, M. O.: Correlation between cloud condensation nuclei concentration and aerosol optical thickness in remote and polluted regions, Atmospheric Chemistry and Physics, 9, 543–556, https://doi.org/10.5194/acp-9-543-2009, https://www.atmos-chem-phys.net/9/543/2009/, 2009.

Andreae, M. O., Rosenfeld, D., Artaxo, P., Costa, A., Frank, G., Longo, K., and Silva-Dias, M.: Smoking rain clouds over the Amazon, Science, 303, 1337–1342, 2004.

345 Andreae, M. O., Afchine, A., Albrecht, R., Holanda, B. A., Artaxo, P., Barbosa, H. M. J., Borrmann, S., Cecchini, M. A., Costa, A., Dollner, M., Fütterer, D., Järvinen, E., Jurkat, T., Klimach, T., Konemann, T., Knote, C., Krämer, M., Krisna, T., Machado, L. A. T., Mertes, S., Minikin, A., Pöhlker, C., Pöhlker, M. L., Pöschl, U., Rosenfeld, D., Sauer, D., Schlager, H., Schnaiter, M., Schneider, J., Schulz, C., Spanu, A., Sperling, V. B., Voigt, C., Walser, A., Wang, J., Weinzierl, B., Wendisch, M., and Ziereis, H.: Aerosol characteristics and particle production in the upper troposphere over the Amazon Basin, Atmospheric Chemistry and Physics, 18, 921–961, https://doi.org/10.5194/acp-
350 18-921-2018, https://www.atmos-chem-phys.net/18/921/2018/, 2018.

Archer-Nicholls, S., Lowe, D., Schultz, D. M., and McFiggans, G.: Aerosol–radiation–cloud interactions in a regional coupled model: the effects of convective parameterisation and resolution, Atmospheric Chemistry and Physics, 16, 5573, 2016.

Barnard, J. C., Fast, J. D., Paredes-Miranda, G., Arnott, W. P., and Laskin, A.: Technical Note: Evaluation of the WRF-Chem "Aerosol Chemical to Aerosol Optical Properties" Module using data from the MILAGRO campaign, Atmospheric Chemistry and Physics, 10,
355 7325–7340, https://doi.org/10.5194/acp-10-7325-2010, 2010.

Baumgardner, D., Brenguier, J., Bucholtz, A., Coe, H., DeMott, P., Garrett, T., Gayet, J., Hermann, M., Heymsfield, A., Korolev, A., et al.: Airborne instruments to measure atmospheric aerosol particles, clouds and radiation: A cook's tour of mature and emerging technology, Atmospheric Research, 102, 10–29, 2011.

Baumgardner, D., Newton, R., Krämer, M., Meyer, J., Beyer, A., Wendisch, M., and Vochezer, P.: The Cloud Particle Spectrometer with
360 Polarization Detection (CPSPD): A next generation open-path cloud probe for distinguishing liquid cloud droplets from ice crystals, Atmospheric Research, 142, 2–14, 2014.

Braga, R. C., Rosenfeld, D., Weigel, R., Jurkat, T., Andreae, M. O., Wendisch, M., Pöhlker, M. L., Klimach, T., Pöschl, U., Pöhlker, C., Voigt, C., Mahnke, C., Borrmann, S., Albrecht, R. I., Molleker, S., Vila, D. A., Machado, L. A. T., and Artaxo, P.: Comparing parameterized versus measured microphysical properties of tropical convective cloud bases during the ACRIDICON–CHUVA campaign, Atmospheric
365 Chemistry and Physics, 17, 7365–7386, https://doi.org/10.5194/acp-17-7365-2017, 2017a.

Braga, R. C., Rosenfeld, D., Weigel, R., Jurkat, T., Andreae, M. O., Wendisch, M., Pöschl, U., Voigt, C., Mahnke, C., Borrmann, S., et al.: Further evidence for CCN aerosol concentrations determining the height of warm rain and ice initiation in convective clouds over the Amazon basin, Atmospheric Chemistry and Physics, 17, 14 433–14 456, 2017b.

Brioude, J., Cooper, O., Feingold, G., Trainer, M., Freitas, S., Kowal, D., Ayers, J., Prins, E., Minnis, P., McKeen, S., et al.: Effect of biomass
370 burning on marine stratocumulus clouds off the California coast, Atmospheric Chemistry and Physics, 9, 8841–8856, 2009.

Chapman, E. G., Gustafson Jr, W., Easter, R. C., Barnard, J. C., Ghan, S. J., Pekour, M. S., and Fast, J. D.: Coupling aerosol-cloud-radiative processes in the WRF-Chem model: Investigating the radiative impact of elevated point sources, Atmospheric Chemistry and Physics, 9, 945–964, 2009.

Emmons, L. K., Walters, S., Hess, P. G., Lamarque, J.-F., Pfister, G. G., Fillmore, D., Granier, C., Guenther, A., Kinnison, D., Laepple, T., Orlando, J., Tie, X., Tyndall, G., Wiedinmyer, C., Baughcum, S. L., and Kloster, S.: Description and evaluation of the Model for Ozone and Related chemical Tracers, version 4 (MOZART-4), Geoscientific Model Development, 3, 43–67, https://doi.org/10.5194/gmd-3-43-2010, 2010.

Ewald, F., Kölling, T., Baumgartner, A., Zinner, T., and Mayer, B.: Design and characterization of specMACS, a multipurpose hyperspectral cloud and sky imager, Atmospheric Measurement Techniques, pp. 2015–2042, 2016.

Ewald, F., Zinner, T., Kölling, T., and Mayer, B.: Remote Sensing of Cloud Droplet Radius Profiles using solar reflectance from cloud sides. Part I: Retrieval development and characterization, Atmospheric Measurement Techniques Discussions, 2018, 1–35, https://doi.org/10.5194/amt-2018-234, 2018.

Fast, J. D., Gustafson Jr, W. I., Easter, R. C., Zaveri, R. A., Barnard, J. C., Chapman, E. G., Grell, G. A., and Peckham, S. E.: Evolution of ozone, particulates, and aerosol direct radiative forcing in the vicinity of Houston using a fully coupled meteorology-chemistry-aerosol model, Journal of Geophysical Research: Atmospheres, 111, 2006.

Flamant, C., Knippertz, P., Fink, A. H., Akpo, A., Brooks, B., Chiu, C. J., Coe, H., Danuor, S., Evans, M., Jegede, O., et al.: The Dynamics–Aerosol–Chemistry–Cloud Interactions in West Africa Field Campaign: Overview and Research Highlights, Bulletin of the American Meteorological Society, 99, 83–104, 2018.

Freud, E., Rosenfeld, D., and Kulkarni, J.: Resolving both entrainment-mixing and number of activated CCN in deep convective clouds, Atmospheric Chemistry and Physics, 11, 12 887–12 900, 2011.

Grell, G. A., Peckham, S. E., Schmitz, R., McKeen, S. A., Frost, G., Skamarock, W. C., and Eder, B.: Fully coupled "online" chemistry within the WRF model, Atmospheric Environment, 39, 6957–6975, 2005.

Grosvenor, D. P., Sourdeval, O., Zuidema, P., Ackerman, A., Alexandrov, M. D., Bennartz, R., Boers, R., Cairns, B., Chiu, J. C., Christensen, M., Deneke, H., Diamond, M., Feingold, G., Fridlind, A., Hünerbein, A., Knist, C., Kollias, P., Marshak, A., McCoy, D., Merk, D., Painemal, D., Rausch, J., Rosenfeld, D., Russchenberg, H., Seifert, P., Sinclair, K., Stier, P., van Diedenhoven, B., Wendisch, M., Werner, F., Wood, R., Zhang, Z., and Quaas, J.: Remote Sensing of Droplet Number Concentration in Warm Clouds: A Review of the Current State of Knowledge and Perspectives, Reviews of Geophysics, 56, 409–453, https://doi.org/10.1029/2017RG000593, 2018.

Guenther, A., Karl, T., Harley, P., Wiedinmyer, C., Palmer, P., and Geron, C.: Estimates of global terrestrial isoprene emissions using MEGAN (Model of Emissions of Gases and Aerosols from Nature), Atmospheric Chemistry and Physics, 6, 3181–3210, 2006.

Gustafson Jr, W. I., Chapman, E. G., Ghan, S. J., Easter, R. C., and Fast, J. D.: Impact on modeled cloud characteristics due to simplified treatment of uniform cloud condensation nuclei during NEAQS 2004, Geophysical Research Letters, 34, 2007.

IPCC: Climate Change 2014: Synthesis Report. Contribution of Working Groups I, II and III to the Fifth Assessment Report of the Intergovernmental Panel on Climate Change, IPCC, Geneva, Switzerland, 2014.

Jäkel, E., Wendisch, M., Krisna, T. C., Ewald, F., Kölling, T., Jurkat, T., Voigt, C., Cecchini, M. A., Machado, L. A. T., Afchine, A., Costa, A., Krämer, M., Andreae, M. O., Pöschl, U., Rosenfeld, D., and Yuan, T.: Vertical distribution of the particle phase in tropical deep convective clouds as derived from cloud-side reflected solar radiation measurements, Atmospheric Chemistry and Physics, 17, 9049–9066, https://doi.org/10.5194/acp-17-9049-2017, 2017.

Janssens-Maenhout, G., Dentener, F., Van Aardenne, J., Monni, S., Pagliari, V., Orlandini, L., Klimont, Z., Kurokawa, J.-i., Akimoto, H., Ohara, T., et al.: EDGAR-HTAP: a harmonized gridded air pollution emission dataset based on national inventories, European Commission Joint Research Centre Institute for Environment and Sustainability. JRC 68434 UR 25229 EUR 25229, ISBN 978-92-79-23123-0, 2012.

Järvinen, E., Schnaiter, M., Mioche, G., Jourdan, O., Shcherbakov, V. N., Costa, A., Afchine, A., Krämer, M., Heidelberg, F., Jurkat, T., et al.: Quasi-spherical ice in convective clouds, Journal of the Atmospheric Sciences, 73, 3885–3910, 2016.

Kleine, J., Voigt, C., Sauer, D., Schlager, H., Scheibe, M., Jurkat-Witschas, T., Kaufmann, S., Kärcher, B., and Anderson, B. E.: In Situ Observations of Ice Particle Losses in a Young Persistent Contrail, Geophysical Research Letters, 45, 13,553–13,561, https://doi.org/10.1029/2018GL079390, 2018.

Knote, C., Hodzic, A., Jimenez, J. L., Volkamer, R., Orlando, J. J., Baidar, S., Brioude, J., Fast, J., Gentner, D. R., Goldstein, A. H., Hayes, P. L., Knighton, W. B., Oetjen, H., Setyan, A., Stark, H., Thalman, R., Tyndall, G., Washenfelder, R., Waxman, E., and Zhang, Q.: Simulation of semi-explicit mechanisms of SOA formation from glyoxal in aerosol in a 3-D model, Atmospheric Chemistry and Physics, 14, 6213–6239, https://doi.org/10.5194/acp-14-6213-2014, 2014.

Knote, C., Hodzic, A., and Jimenez, J. L.: The effect of dry and wet deposition of condensable vapors on secondary organic aerosols concentrations over the continental US, Atmospheric Chemistry and Physics, 15, 1–18, https://doi.org/10.5194/acp-15-1-2015, 2015.

Krüger, M. L., Mertes, S., Klimach, T., Cheng, Y. F., Su, H., Schneider, J., Andreae, M. O., Pöschl, U., and Rose, D.: Assessment of cloud supersaturation by size-resolved aerosol particle and cloud condensation nuclei (CCN) measurements, Atmospheric Measurement Techniques, 7, 2615–2629, https://doi.org/10.5194/amt-7-2615-2014, 2014.

Lance, S., Brock, C., Rogers, D., and Gordon, J. A.: Water droplet calibration of the Cloud Droplet Probe (CDP) and in-flight performance in liquid, ice and mixed-phase clouds during ARCPAC, Atmospheric Measurement Techniques, 3, 1683–1706, 2010.

Levin, Z., Teller, A., Ganor, E., and Yin, Y.: On the interactions of mineral dust, sea-salt particles, and clouds: A measurement and modeling study from the Mediterranean Israeli Dust Experiment campaign, Journal of Geophysical Research: Atmospheres, 110, 2005.

Malavelle, F. F., Haywood, J. M., Jones, A., Gettelman, A., Clarisse, L., Bauduin, S., Allan, R. P., Karset, I. H. H., Kristjánsson, J. E., Oreopoulos, L., et al.: Strong constraints on aerosol–cloud interactions from volcanic eruptions, Nature, 546, 485, 2017.

Marshak, A., Platnick, S., Várnai, T., Wen, G., and Cahalan, R. F.: Impact of three-dimensional radiative effects on satellite retrievals of cloud droplet sizes, Journal of Geophysical Research: Atmospheres, 111, 2006.

Martins, J. A., Silva Dias, M. A. F., and Gonçalves, F. L. T.: Impact of biomass burning aerosols on precipitation in the Amazon: A modeling case study, Journal of Geophysical Research: Atmospheres, 114, https://doi.org/10.1029/2007JD009587, 2009.

Martins, J. V., Marshak, A., Remer, L., Rosenfeld, D., Kaufman, Y., Fernandez-Borda, R., Koren, I., Correia, A. L., Zubko, V., and Artaxo, P.: Remote sensing the vertical profile of cloud droplet effective radius, thermodynamic phase, and temperature, Atmospheric Chemistry and Physics, 11, 9485–9501, 2011.

McCoy, D. T. and Hartmann, D. L.: Observations of a substantial cloud-aerosol indirect effect during the 2014–2015 Baroarbunga-Veioivotn fissure eruption in Iceland, Geophysical Research Letters, 42, 10–409, 2015.

Morrison, H. and Gettelman, A.: A new two-moment bulk stratiform cloud microphysics scheme in the Community Atmosphere Model, version 3 (CAM3). Part I: Description and numerical tests, Journal of Climate, 21, 3642–3659, 2008.

Morrison, H., Curry, J., and Khvorostyanov, V.: A new double-moment microphysics parameterization for application in cloud and climate models. Part I: Description, Journal of the Atmospheric Sciences, 62, 1665–1677, 2005.

Morrison, H., Thompson, G., and Tatarskii, V.: Impact of cloud microphysics on the development of trailing stratiform precipitation in a simulated squall line: Comparison of one-and two-moment schemes, Monthly Weather Review, 137, 991–1007, 2009.

Pöhlker, M. L., Ditas, F., Saturno, J., Klimach, T., Hrabě de Angelis, I., Araùjo, A. C., Brito, J., Carbone, S., Cheng, Y., Chi, X., Ditz, R., Gunthe, S. S., Holanda, B. A., Kandler, K., Kesselmeier, J., Könemann, T., Krüger, O. O., Lavrič, J. V., Martin, S. T., Mikhailov, E., Moran-Zuloaga, D., Rizzo, L. V., Rose, D., Su, H., Thalman, R., Walter, D., Wang, J., Wolff, S., Barbosa, H. M. J., Artaxo, P., Andreae, M. O., Pöschl, U., and Pöhlker, C.: Long-term observations of cloud condensation nuclei over the Amazon rain forest – Part 2: Variability
450   and characteristics of biomass burning, long-range transport, and pristine rain forest aerosols, Atmospheric Chemistry and Physics, 18, 10 289–10 331, https://doi.org/10.5194/acp-18-10289-2018, 2018.

Reid, J. S., Hobbs, P. V., Rangno, A. L., and Hegg, D. A.: Relationships between cloud droplet effective radius, liquid water content, and droplet concentration for warm clouds in Brazil embedded in biomass smoke, Journal of Geophysical Research: Atmospheres, 104, 6145–6153, 1999.

455   Roberts, G. and Nenes, A.: A continuous-flow streamwise thermal-gradient CCN chamber for atmospheric measurements, Aerosol Science and Technology, 39, 206–221, 2005.

Rose, D., Gunthe, S., Mikhailov, E., Frank, G., Dusek, U., Andreae, M. O., and Pöschl, U.: Calibration and measurement uncertainties of a continuous-flow cloud condensation nuclei counter (DMT-CCNC): CCN activation of ammonium sulfate and sodium chloride aerosol particles in theory and experiment, Atmospheric Chemistry and Physics, 8, 1153–1179, 2008.

460   Rosenfeld, D.: TRMM observed first direct evidence of smoke from forest fires inhibiting rainfall, Geophysical Research Letters, 26, 3105–3108, 1999.

Rosenfeld, D., Williams, E., Andreae, M., Freud, E., Pöschl, U., and Rennó, N.: The scientific basis for a satellite mission to retrieve CCN concentrations and their impacts on convective clouds, Atmospheric Measurement Techniques, 5, 2039–2055, 2012.

Sassen, K., DeMott, P. J., Prospero, J. M., and Poellot, M. R.: Saharan dust storms and indirect aerosol effects on clouds: CRYSTAL-FACE
465   results, Geophysical Research Letters, 30, 2003.

Schumann, U., Baumann, R., Baumgardner, D., Bedka, S. T., Duda, D. P., Freudenthaler, V., Gayet, J.-F., Heymsfield, A. J., Minnis, P., Quante, M., Raschke, E., Schlager, H., Vázquez-Navarro, M., Voigt, C., and Wang, Z.: Properties of individual contrails: a compilation of observations and some comparisons, Atmospheric Chemistry and Physics, 17, 403–438, https://doi.org/10.5194/acp-17-403-2017, 2017.

Seinfeld, J. H., Bretherton, C., Carslaw, K. S., Coe, H., DeMott, P. J., Dunlea, E. J., Feingold, G., Ghan, S., Guenther, A. B., Kahn, R., et al.:
470   Improving our fundamental understanding of the role of aerosol- cloud interactions in the climate system, Proceedings of the National Academy of Sciences, 113, 5781–5790, 2016.

Taylor, J. W., Haslett, S. L., Bower, K., Flynn, M., Crawford, I., Dorsey, J., Choularton, T., Connolly, P. J., Hahn, V., Voigt, C., et al.: Aerosol influences on low-level clouds in the West African monsoon, Atmos. Chem. Phys. Discuss., https://doi. org/10.5194/acp-2019-40, in review, 2019.

475   Thompson, G., Field, P. R., Rasmussen, R. M., and Hall, W. D.: Explicit forecasts of winter precipitation using an improved bulk microphysics scheme. Part II: Implementation of a new snow parameterization, Monthly Weather Review, 136, 5095–5115, 2008.

Twomey, S.: Aerosols, clouds and radiation, Atmospheric Environment. Part A. General Topics, 25, 2435–2442, 1991.

Voigt, C., Schumann, U., Minikin, A., Abdelmonem, A., Afchine, A., Borrmann, S., Boettcher, M., Buchholz, B., Bugliaro, L., Costa, A., et al.: ML-CIRRUS: The airborne experiment on natural cirrus and contrail cirrus with the high-altitude long-range research aircraft
480   HALO, Bulletin of the American Meteorological Society, 98, 271–288, 2017.

Weigel, R., Spichtinger, P., Mahnke, C., Klingebiel, M., Afchine, A., Petzold, A., Krämer, M., Costa, A., Molleker, S., Reutter, P., Szakáll, M., Port, M., Grulich, L., Jurkat, T., Minikin, A., and Borrmann, S.: Thermodynamic correction of particle concentrations measured by

underwing probes on fast-flying aircraft, Atmospheric Measurement Techniques, 9, 5135–5162, https://doi.org/10.5194/amt-9-5135-2016, 2016.

485 Wendisch, M., Pöschl, U., Andreae, M. O., Machado, L. A., Albrecht, R., Schlager, H., Rosenfeld, D., Martin, S. T., Abdelmonem, A., Afchine, A., et al.: ACRIDICON–CHUVA campaign: Studying tropical deep convective clouds and precipitation over Amazonia using the new German research aircraft HALO, Bulletin of the American Meteorological Society, 97, 1885–1908, 2016.

Wiedinmyer, C., Akagi, S., Yokelson, R. J., Emmons, L., Al-Saadi, J., Orlando, J., and Soja, A.: The Fire INventory from NCAR (FINN): A high resolution global model to estimate the emissions from open burning, Geoscientific Model Development, 4, 625, 2011.

490 Wu, L., Su, H., and Jiang, J. H.: Regional simulations of deep convection and biomass burning over South America: 2. Biomass burning aerosol effects on clouds and precipitation, Journal of Geophysical Research: Atmospheres, 116, https://doi.org/10.1029/2011JD016106, 2011.

Wyngaard, J. C.: Toward Numerical Modeling in the "Terra Incognita", Journal of the Atmospheric Sciences, 61, 1816–1826, https://doi.org/10.1175/1520-0469(2004)061<1816:TNMITT>2.0.CO;2, 2004.

495 Zaveri, R. A., Easter, R. C., Fast, J. D., and Peters, L. K.: Model for simulating aerosol interactions and chemistry (MOSAIC), Journal of Geophysical Research: Atmospheres, 113, 2008.

Zhang, Y., Wen, X.-Y., and Jang, C.: Simulating chemistry–aerosol–cloud–radiation–climate feedbacks over the continental US using the online-coupled Weather Research Forecasting Model with chemistry (WRF/Chem), Atmospheric Environment, 44, 3568–3582, 2010.

Zinner, T., Marshak, A., Lang, S., Martins, J., and Mayer, B.: Remote sensing of cloud sides of deep convection: towards a three-dimensional 500 retrieval of cloud particle size profiles, Atmospheric Chemistry and Physics, 8, 4741–4757, 2008.